Light Curve Asymmetries in Three Short Period Eclipsing Binary Stars

Gage Hahs
Charlyn Ortmann
Vayujeet Gokhale
Truman State University, Department of Physics, Kirksville, MO 63501; gokhale@truman.edu

Received February 19, 2020; revised April 10, 2020; accepted April 23, 2020

Abstract We present light curve analysis of three variable stars, NSVS 10384295 (P = 0.297899 d), NSVS 7347726 (P = 0.43394 d), and NSVS 13251721 (P = 0.23340 d), using data collected at the 31-inch NURO telescope at the Lowell Observatory in Flagstaff, Arizona, in three filters: Bessell B, V, and R. We quantify the asymmetries in these systems by generating a twelve-term Fourier fit and using the resulting Fourier coefficients to calculate ΔI (the difference in the heights of the primary and secondary maxima), the "Light Curve Asymmetry" (LCA), and the "O'Connell Effect Ratio" (OER). Our analysis shows that of the three systems studied, NSVS 13251721 has the most asymmetric light curve, and that NSVS 7347726 has the most symmetric light curve. We also observe that for all three systems, the asymmetries are most pronounced in the B filter, and the least in the R filter. Additionally, we use the Fourier coefficients to confirm NSVS 10384295 and NSVS 13251721 as W UMa type systems, and NSVS 7347726 to be a β Lyrae type system.

1. Introduction

We present results for three eclipsing binary systems selected from Hoffman *et al.* (2008), namely, NSVS 10384295 (P = 0.297899d), NSVS 7347726 (P = 0.43394d), and NSVS 13251721 (P = 0.23340d). This project is part of an effort at Truman State University to introduce undergraduate students to differential aperture photometry by following three to four eclipsing binaries per semester with the aim of generating light curves, classifying these systems as either β Lyrae, Algol, or W UMa type systems, and quantifying the asymmetries in the light curves of these objects. Following Gardner *et al.* (2015) and Akiba *et al.* (2019), we focus on the asymmetries in the light curves in each of the filters by calculating the difference in the heights of the primary and secondary maxima (ΔI), the "Light Curve Asymmetry" (LCA), and the "O'Connell Effect Ratio" (OER; McCartney 1999; O'Connell 1951). The OER is the ratio of the area under the curves between phases φ = 0.0 to φ = 0.5 and phases φ = 0.5 to φ = 1.0 (see section 3 below). An OER > 1 implies that the first half of the light curve has more total flux than the second half. The LCA, on the other hand, measures the deviance from symmetry of the two halves of the light curve. If both halves are perfectly symmetric, then we would expect the LCA to be zero. We refer the reader to Gardner *et al.* (2015) for a more detailed discussion on the LCA and OER. We are interested in studying these asymmetries since their origin is not well studied or understood—the two most popular explanations, the "starspot" model and the "hotspot" model, are not entirely satisfactory (Akiba *et al.* 2019).

We do not attempt to model these systems—that would require access to spectroscopic data, which we do not have. Instead, we superpose the two halves of an appropriately phased light curve to identify the phase at which the light curves are asymmetric (see section 3). In the starspot model, this phase information can be used to constrain the location and characteristics of the starspots for a given orbital cycle. This, however, has limited utility given that astronomers usually only have one or two orbital cycles of data. We are working on using uninterrupted data from the Kepler (Prša *et al.* 2011) and Transiting Exoplanet Survey Satellite (TESS) missions (Ricker *et al.* 2015) to constrain the system parameters even without access to spectroscopic data. In particular, we aim to investigate the time evolution of "starspots" on the surface of one, or both, components in the binary system. From this, we want to determine what role these starspots play in the observed, and as yet, not well understood asymmetries in the light curves of eclipsing binary star systems.

In the following, section 2 outlines our observational data acquisition and data reduction methods, section 3 contains our results and analysis of the light curves, and section 4 is a discussion of our results.

2. Observations

We present BVR photometry of eclipsing variable stars NSVS 10384295 (P = 0.297899 d), NSVS 7347726 (P = 0.43394 d), and NSVS 13251721 (P = 0.23340 d). The data were collected using the 2 k × 2 k Loral NASACam CCD attached to the 31-inch NURO telescope at Lowell Observatory, Flagstaff, Arizona. The filters used are Bessell BVR (see Table 1). We follow the procedure outlined in Gardner *et al.* (2015) for data collection and reduction: Bias subtraction and

Table 1. Observation dates, instrument, and filters for the targets.

Target	*Date of Observation*	*Telescope*	*Filters*
NSVS 10384295	08 March 2016	NURO	Bessell BVR
	09 March 2016	NURO	Bessell BVR
NSVS 7347726	09 March 2016	NURO	Bessell BVR
	10 March 2016	NURO	Bessell BVR
	11 March 2016	NURO	Bessell BVR
NSVS 13251721	10 March 2016	NURO	Bessell BVR
	10 March 2016	NURO	Bessell BVR

Table 2. Target, comparison, and check star coordinates and comparison star B and V magnitudes used for data from the NURO telescope.

Star	*Name*	*R.A. (J2000)* h m s	*Dec. (J2000)* ° ′ ″	*V*	*B*
Target	NSVS 10384295	12 32 49.94	+15 17 35.21		
Comparison	BD+16 2388	12 32 39.29	+15 13 36.83	10.4	11.5
Check	BD+16 2387	12 32 28.36	+15 18 19.49		
Target	NSVS 7347726	08 08 57.97	+37 12 05.62		
Comparison	TYC 2481-548-1	08 08 42.65	+37 09 08.45	12.10	12.73
Check	TYC 2481-26-1	08 08 32.02	+37 06 14.04		
Target	NSVS 13251721	13 32 28.07	–02 30 56.52		
Comparison	UCAC2 30863052	13 32 02.04	–02 33 13.11	11.877	12.517
Check	—	13 32 02.45	–02 33 51.20		

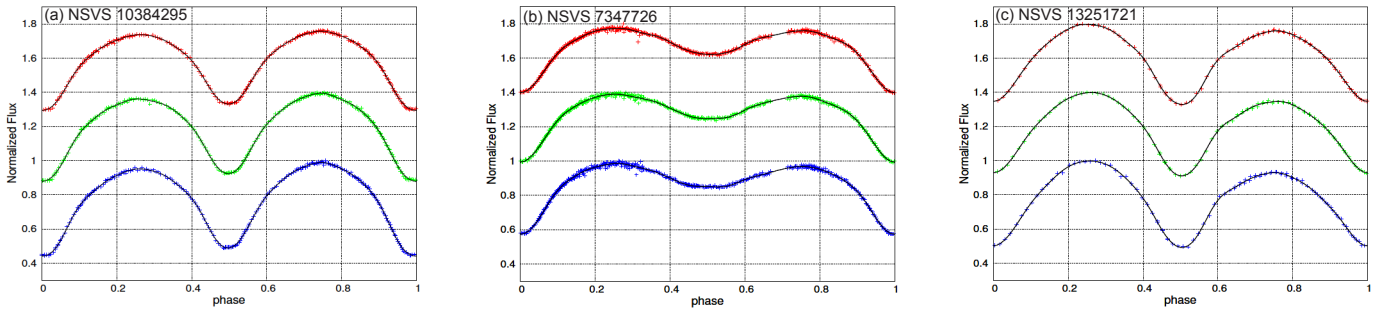

Figure 1. Differential magnitudes ("+" symbols) for each of the systems. The Fourier fit (black continuous curve) is plotted along with the red, green, and blue curves corresponding to R, V, and B filters, respectively. Note that these curves are generated after the data for each object had been shifted so that the primary eclipse occurs at phase 0. The average error in flux for NSVS 10384295 and NSVS 13251721 in each of the three filters is about 0.007, and for NSVS 7347726 it is about 0.01. Error bars are not shown for the sake of clarity.

Table 3. Classification of systems based on Fourier coefficients.

Target	*Filter*	a_1	a_2	a_4	$a_2(0.125–a_2)$	*Classification*
NSVS 10384295	B	0.0301 ± 0.0005	–0.2367 ± 0.0005	–0.0577 ± 0.0005	–0.0856 ± 0.0002	W UMa
	V	0.0268 ± 0.0005	–0.2225 ± 0.0006	–0.0556 ± 0.0005	–0.0773 ± 0.0002	W UMa
	R	0.0227 ± 0.0005	–0.2039 ± 0.0005	–0.0511 ± 0.0005	–0.0670 ± 0.0002	W UMa
NSVS 7347726	B	0.0780 ± 0.0004	–0.1248 ± 0.0005	–0.0267 ± 0.0005	–0.0312 ± 0.0001	β Lyrae
	V	0.0726 ± 0.0003	–0.1234 ± 0.0004	–0.0269 ± 0.0004	–0.0306 ± 0.0001	β Lyrae
	R	0.0636 ± 0.0003	–0.1203 ± 0.0004	–0.0272 ± 0.0004	–0.0295 ± 0.0001	β Lyrae
NSVS 13251721	B	0.0083 ± 0.0009	–0.2199 ± 0.0009	–0.0441 ± 0.0010	–0.0759 ± 0.0004	W UMa
	V	0.0022 ± 0.0006	–0.2119 ± 0.0006	–0.0446 ± 0.0007	–0.0714 ± 0.0003	W UMa
	R	–0.0023 ± 0.0007	–0.2066 ± 0.0006	–0.0436 ± 0.0007	–0.0685 ± 0.0003	W UMa

(sky) flat fielding is done using the software package MAXIMDL (v6.16; Diffraction Limited 2020). No dark subtraction was performed since for the nitrogen cooled camera at NURO, the dark current is negligible. Differential photometry is then performed on the target with a suitable comparison and check star using the ASTROIMAGEJ software (v3.2; Collins *et al.* 2017) (Differential photometry data are available on request via email: gokhale@truman.edu and at http://gokhale.sites.truman.edu/asymmetries/.) The aperture size was set to two times the full width at half maximum (FWHM) of the brightest object on which photometry was performed. The radius of the inner annulus was chosen to exclude any other stars close to the target, whilst the outer radius was set to ensure that the annulus contains approximately 4 times the number of pixels that are in the aperture, following the procedure outlined by Conti (2018). We searched for any comparison stars from the Tycho (Høg *et al.* 2000) catalogue that are present in the image frame, and used these stars to determine the B and V magnitudes of each of the targets. Since we could not find the R magnitude of any of the comparison stars, differential photometry was performed on the R-filter data using instrumental magnitudes. The details for the target, comparison, and check star are provided in Table 2.

3. Results and analyses

3.1. Light curves

We phase fold the time axis of each of the light curves using the equation:

$$\Phi = \frac{T - T_0}{P} - \text{Int}\quad\frac{T - T_0}{P} \tag{1}$$

where P is the period of the system (Hoffman *et al.* 2008) and T_0 is an arbitrarily chosen epoch. Following Warner and Harris (2006), we convert the differential magnitude measured in each filter to the normalized flux by using:

$$I(\Phi)_{\text{obs}} = 10^{-0.4 \times (m(\Phi) - m(\max))} \tag{2}$$

where $m(\Phi)$ is the magnitude at a certain phase Φ and $m(\max)$ is the maximum magnitude observed for the object. We perform Fourier fit analyses on the light curves by generating a truncated twelve-term Fourier fit (Wilsey and Beaky 2009):

$$I(\Phi)_{\text{fit}} = a_0 + \sum_{n=1}^{12}(a_n \cos(2\pi n\Phi) + b_n \sin(2\pi n\Phi)) \tag{3}$$

where a_0, a_n, and b_n are the Fourier coefficients of the fit, and Φ is the phase (Hoffman *et al.* 2009). Note that the Fourier fit is accomplished using WOLFRAM MATHEMATICA (Wolfram Res. Co. 2019). The phase-folded light curves, along with the corresponding Fourier fits, are shown in Figures 1a, 1b and 1c.

3.2. Classification of systems

We follow the procedure outlined by Rucinski (1997) and Wiley and Beaky (2009) and summarized in Akiba *et al.* (2019) (see their section 3.2) to classify the three systems under consideration. The Fourier coefficients, and the associated errors, are extracted from the Fourier fits generated using MATHEMATICA (Wolfram Res. Co. 2019) and are tabulated in Table 3. Each filter gives us consistent results which match with the expected classification based on a visual inspection of the light curves: NSVS 10384295 and NSVS 13251721 are confirmed to be of the W UMa type, whilst NSVS 7347726 is confirmed to be of the β Lyrae type.

3.3. Asymmetries in the light curve: Quantifying the O'Connell Effect

We again follow the procedure outlined by Akiba *et al.* (2019) to quantify the asymmetries in the light curves of each of these objects in each filter. We first calculate the difference in the normalized flux near the primary and secondary maxima as ΔI_{ave} and ΔI_{fit} using our data and fit, respectively. Also, the coefficient b_1 associated with the first sine term of the Fourier fit is the half-amplitude of the sine wave, and therefore $|2b_1|$ is a good approximation to ΔI (Wilsey and Beaky 2009). The calculated values of $|2b_1|$, ΔI (Fourier), andΔI (Average) are shown in Table4.

Then, we evaluate the O'Connell Effect Ratio (OER) and the Light Curve Asymmetry (LCA) as described by McCartney (1999) as follows:

$$\text{OER} = \frac{\int_{0.0}^{0.5}(I(\Phi)_{\text{fit}} - I(0.0)_{\text{fit}})d\Phi}{\int_{0.5}^{1.0}(I(\Phi)_{\text{fit}} - I(0.0)_{\text{fit}})d\Phi} \tag{4}$$

and,

$$\text{LCA} = \sqrt{\int_{0.0}^{0.5}\frac{(I(\Phi)_{\text{fit}} - I(1.0 - \Phi)_{\text{fit}})^2}{I(\Phi)^2_{\text{fit}}}\,d\Phi} \tag{5}$$

where $I(\Phi)_{\text{fit}}$ is given by Equation 3. The values for these parameters are tabulated in Table 5. The uncertainties of the OER and LCA are calculated according to the formal proofs outlined in the appendices of Akiba *et al.* (2019).

It is instructive to superpose the two halves of an eclipsing binary light curve to visually appreciate the asymmetries in them. In addition, we calculate the difference in the two halves of the light curve as:

$$\Delta I(\Phi)_{\text{fit}} = I(\Phi)_{\text{fit}} - I(1 - \Phi)_{\text{fit}} \tag{6}$$

Figure 2 shows the "half-phase plot" for each of our systems in the B filter. The $\Delta I(\Phi)_{\text{fit}}$ function is plotted in the bottom panel. Figure 3 shows the difference in the two halves of the light curve in each of the filters for all the three systems under consideration. The plots show certain similarities in the asymmetries in the three filters. For example, in all three filters $\Delta I(\Phi)_{\text{fit}}$ is largely negative for NSVS 10384295, in keeping with the fact that the maxima after the secondary eclipse is brighter than the maximum after the primary eclipse for this system. $\Delta I(\Phi)_{\text{fit}}$ values for NSVS 7347726 and NSVS 13251721 are largely positive, with the latter showing a significantly larger asymmetry than the former system. It is also clear that the discrepancy in flux is greatest in the B filter and least in the R filter, which is also a trend we notice in other asymmetry parameters like the OER, LCA, and the ΔIs.

As mentioned earlier, we are in the process of generating similar plots and animations for eclipsing binary systems over several orbital cycles using data obtained from the TESS and Kepler missions. This will allow us to study the changes in the asymmetry as a function of time, which will be valuable in modeling these systems (Koogler *et al.* 2019).

4. Discussion

4.1. NSVS 10384295

From Table 3 for NSVS 10384295, we see that $a_4 > I_2(0.125 - a_2)$ in all filters, which suggests that the system is an overcontact W UMa or β Lyrae type eclisping binary system. Since $|a_1| < 0.05$ in all filters we classify NSVS 10384295 as a W UMa type system, following the criteria summarized in Akiba *et al.* (2019). This is consistent with the shape of its light curve (Figure 1a).

By visual inspection of the light curve, we see that NSVS 10384295 exhibits the O'Connell Effect with the peak magnitude after the primary eclipse being less than the peak magnitude after the secondary eclipse. This is reflected in the negative ΔI values in Table 4. Similarly, the OER is less than 1 for each filter (Table 5), suggesting again that the peak after the secondary eclipse is brighter than the peak after the primary eclipse. Also note that the O'Connell Effect, quantified in terms of ΔI, is most prominent in the B filter and least prominent in the R filter (Table 4). This is also reflected in Table 5—the OER

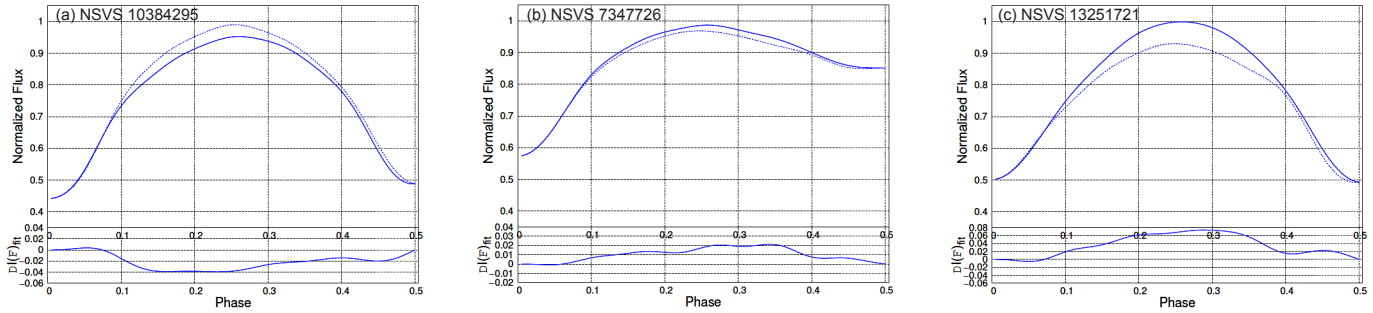

Figure 2. Superposed phased plots of the primary half (solid line) and the secondary half (dotted line) of the light curves in the B filter for each of the systems. The bottom panel shows the difference between the two halves of the light curve. In the absence of any asymmetry, the two curves should coincide, and the solid blue curve in the bottom panel would be a flat line at "0."

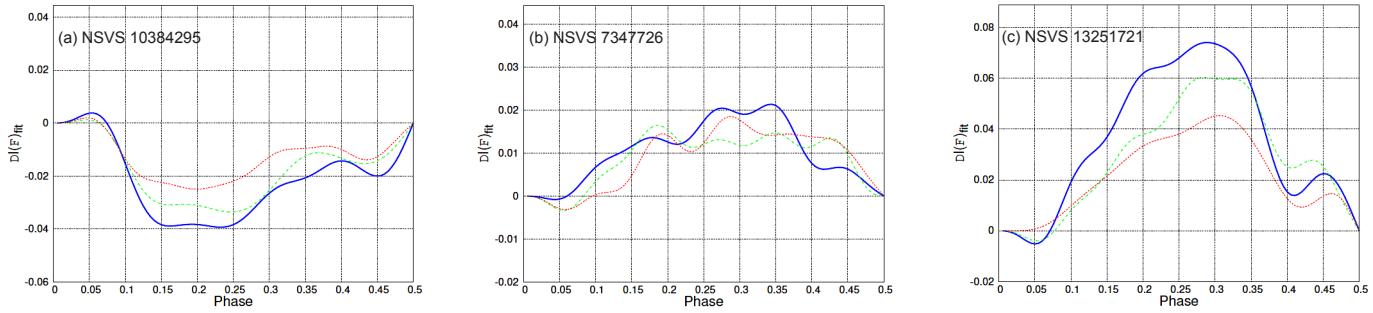

Figure 3. Difference in normalized flux in the B (blue solid curve), V (green dashed), and R (red dotted) filters for each of the systems. See text for details.

Table 4. Quantifying the O'Connell Effect in terms of difference in maxima.

Target	*Filter*	$\|2b_1\|$	*ΔI (Fourier)*	*ΔI (Average)*
NSVS 10384295	B	0.034 ± 0.001	–0.037 ± 0.004	–0.036 ± 0.001
	V	0.028 ± 0.001	–0.033 ± 0.004	–0.033 ± 0.002
	R	0.020 ± 0.001	–0.021 ± 0.004	–0.019 ± 0.001
NSVS 7347726	B	0.017 ± 0.001	0.018 ± 0.003	0.017 ± 0.001
	V	0.014 ± 0.001	0.012 ± 0.003	0.013 ± 0.002
	R	0.014 ± 0.001	0.013 ± 0.003	0.014 ± 0.002
NSVS 13251721	B	0.060 ± 0.002	0.069 ± 0.007	0.071 ± 0.004
	V	0.047 ± 0.002	0.052 ± 0.005	0.052 ± 0.003
	R	0.035 ± 0.016	0.038 ± 0.005	0.042 ± 0.002

Table 5. Quantifying the O'Connell Effect in terms of OER and LCA.

Target	*Filter*	*OER*	*LCA*
NSVS 10384295	B	0.938 ± 0.010	0.021 ± 0.002
	V	0.946 ± 0.011	0.017 ± 0.002
	R	0.957 ± 0.012	0.013 ± 0.002
NSVS 7347726	B	1.034 ± 0.011	0.009 ± 0.002
	V	1.031 ± 0.010	0.008 ± 0.001
	R	1.034 ± 0.010	0.008 ± 0.001
NSVS 13251721	B	1.137 ± 0.028	0.033 ± 0.003
	V	1.113 ± 0.021	0.027 ± 0.003
	R	1.087 ± 0.021	0.020 ± 0.003

value deviates from unity the most in the B filter and least in the R filter. Note that the OER is the ratio of the total flux from the object in the "primary" and the `secondary' halves of the light curve (Equation 4), and thus a perfectly symmetric curve corresponds to an OER = 1 (Gardner *et al.* 2015).

4.2. NSVS 7347726

From Table 3 for NSVS 7347726, we see that $a_4 > a_2(0.125 - a_2)$ in each filter, which suggests that the system is either a W UMa or a β Lyrae type system. Inspection of the a_1 coefficient further classifies NSVS 7347726 as a β Lyrae since $a_1 > 0.05$ (Akiba *et al.* 2019). This result based on the Fourier coefficients supports the characteristic β Lyrae light curve shape seen in Figure 1b.

By visual inspection of the light curve, we see that NSVS 7347726 exhibits a less prominent O'Connell Effect with the peak magnitude after the primary eclipse being slightly greater than the peak magnitude after the secondary eclipse. This is reflected by the positive ΔI values in Table 4. Moreover, the difference in maxima (ΔI's, see Table 4) is largest in the B filter and practically identical in the V and R filters. Similarly, the OER and LCA values in the three filters for this object are practically identical. As can be seen in Figure 1b, both maxima, as well as the secondary minimum, are very nearly flat. The OER > 1 consistently in each filter though, allowing us to state that the peak after the primary is greater than the peak after the secondary in magnitude. We note that, in this study, the average LCA for NSVS 7347726 is the smallest of the three objects, which implies a more symmetric light curve.

4.3. NSVS 13251721

For NSVS 13251721, we see that $a_4 > a_2(0.125 - a_2)$, which suggests a close contact W UMa or β Lyrae type system. Additionally, $a_1 < 0.05$, which leads to an overall classification of W UMa that is visually verified through inspection of Figure 1c. Upon further inspection of Figure 1c, we see that NSVS 7347726 exhibits an O'Connell Effect with the peak magnitude after the primary eclipse being greater than the peak magnitude following the secondary eclipse. This is reflected by the positive ΔI values in Table4 and by the OER values in Table 5. Also, we note the familiar pattern where the OER and LCA are most prominent in the B filter and least prominent in the R filter.

5. Acknowledgements

We have made extensive use of the tools avaliable on the AAVSO website, in particular, the VSP (Variable Star Plotter) tool to generate star charts. In addition, we have used the SIMBAD database, operated at CDS, Strasbourg, France, and NASA's Astrophysics Data System. We are thankful for the support provided by the Office of Student Research at Truman State University, and to the Missouri Space Grant Consortium. The authors would also like to thank the anonymous referee for useful comments and suggestions, which greatly improved the manuscript.

References

Akiba, T., Neugarten, A., Ortmann, C., and Gokhale, V. 2019, *J. Amer. Assoc. Var. Star Obs.*, **47**, 186.

Collins, K. A., Kielkopf, J. F., Stassun, K. G., and Hessman, F. V. 2017, *Astron. J.*, **153**, 77.

Conti, D. M. 2018, *A Practical Guide to Exoplanet Observing*, rev. 4.2 (https://astrodennis.com).

Diffraction Limited. 2020 MAXIMDL image processing software (http://www.cyanogen.com).

Gardner, T., Hahs, G., and Gokhale, V. 2015, *J. Amer. Assoc. Var. Star Obs.*, **43**, 186.

Hoffman, D. I., Harrison, T. E., Coughlin, J. L., McNamara, B. J., Holtzman, J. A., Taylor, G. E., and Vestrand, W. T. 2008, *Astron. J.*, **136**, 1067.

Hoffman, D. I., Harrison, T. E., and McNamara, B. J. 2009, *Astron. J.*, **138**, 466.

Høg, E.,*et al.* 2000, *Astron. Astrophys.*, **355**, L27.

Koogler, B., Shroyer, K., and Gokhale, V. 2019, B*ull. Amer. Astron. Soc.*, **51**, id. 207.02 (aas234-aas.ipostersessions.com/Default.aspx?s=C4-8F-61-93-39-B1-84-E0-B1-57-42-ED-CA-46-8B-77).

McCartney, S. A. 1999, Ph.D. dissertation, University of Oklahoma.

O'Connell, D. J. K. 1951, *Riverview Coll. Obs. Publ.*, **2**, 85.

Prša A.,*et al.* 2011, *Astron. J.*, **141**, 83.

Ricker G. R.,*et al.* 2015, *J. Astron. Telesc. Instrum. Syst.*, **1**, 014003.

Rucinski, S. M. 1997, *Astron. J.*, **113**, 407.

Warner, B. D., and Harris, A. W. 2006 *A Practical Guide to Lightcurve Photometry and Analysis*, Springer, New York.

Wilsey N. J., and Beaky M. M. 2009, in *The Society for Astronomical Sciences 28th Annual Symposium on Telescope Science*, Society for Astronomical Sciences, Rancho Cucamonga, CA, 107.

Wolfram Research Co. 2019, "How to Fit Models with Measurement Errors" (https://reference.wolfram.com/language/howto/FitModelsWithMeasurementErrors.html).